

Dry Reforming of CH₄ Using a Microreactor

Tarsida N. Wedraogo¹, Jing Wu² and Huai Z. Li^{1,*} ¹ Université de Lorraine, CNRS, LRGP, F-54000 Nancy, France; nicolas.wedraogo@univ-lorraine.fr² State Key Joint Laboratory of Environment Simulation and Pollution Control, School of Environment, Tsinghua University, Beijing 100084, China; wu_jing@mail.tsinghua.edu.cn

* Correspondence: huai-zhi.li@univ-lorraine.fr; Tel.: +33-372-743-754

Abstract: In the present study, a comparison of the dry reforming of a gas mixture containing methane, carbon dioxide and nitrogen without contaminants to a ruthenium-based Ru/Al₂O₃ catalyst was carried out in a microreactor for the first time. The influence of the contact time, temperature and composition of the feed on the conversion was exhaustively investigated. The optimal operating conditions were found to be a contact time of 80 milliseconds, a temperature of 700 °C and a CH₄:CO₂ ratio of 1. The assessment of diffusional limitations reveals that there is no resistance to mass transfer, which reveals the potential benefit of the determination of intrinsic reaction kinetics within a microreactor.

Keywords: model biogas conversion; dry reforming; microreactor; syngas; bio-hydrogen; Ru/Al₂O₃ catalyst

1. Introduction

Biogas produced during the anaerobic treatment of wastewater is an interesting energy resource from both an environmental and economic point of view. The intensification of the anaerobic process, such the better control of flow fields and mixing at different scales leads to a higher content of methane in the biogas produced. This has been the subject of investigation by our group for a long time [1–5]. At present, the process of methanization yields biogas composed of 55–70% methane and 30–45% carbon dioxide, along with impurities such as hydrogen sulfide. It can be burned on-site to provide heating or electricity, but there are other value-adding uses. For example, biogas can be processed into synthesis gas (H₂ + CO) through reforming [6–8]. Reforming processes have been used to produce hydrogen from natural gas, usually with the addition of steam, in the so-called steam reforming of methane (SRM) process [9]. In another process, oxygen is added to the methane stream (oxidative methane reforming). In the case of biogas, the carbon dioxide can act as a source of oxygen and the reforming can be carried out without steam, as the dry reforming of methane (DRM), according to the following reaction:



This is a highly endothermic reaction and therefore requires large amounts of heat. However, it has the advantage of simultaneously consuming two greenhouse gases: CO₂ and CH₄. It can be catalyzed by several metals, including Ru, Rh and Ni [10]. Biogas reforming has received increasing interest in recent years. In particular, various catalysts for the DRM have been investigated due to their efficiency and stability, such as Ni-supported catalysts on ZrO₂, La₂O₃–ZrO₂ and CeO₂–ZrO₂ [11], Ni and Ba co-doped La_{0.9}AlO₃ perovskite catalysts [12], Ni/Al catalysts with an egg-shell structure [13], CoNiMgAl catalysts [14], LaCoO₃ and LaNiO₃ perovskite-derived catalysts [15], and Ni-containing CeO₂ rods [16]. Different characterization techniques, including x-ray diffraction (XRD), scanning electron microscopy (SEM), transmission electron microscopy (TEM) and temperature-programmed



Citation: Wedraogo, T.N.; Wu, J.; Li, H.Z. Dry Reforming of CH₄ Using a Microreactor. *Methane* **2024**, *3*, 346–358. <https://doi.org/10.3390/methane3020019>

Academic Editors: Lubomira Tosheva and Patrick Da Costa

Received: 31 January 2024

Revised: 10 May 2024

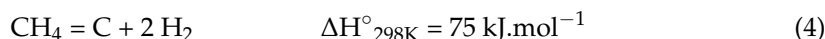
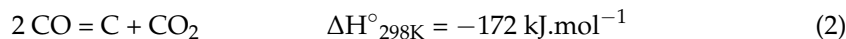
Accepted: 20 May 2024

Published: 3 June 2024



Copyright: © 2024 by the authors. Licensee MDPI, Basel, Switzerland. This article is an open access article distributed under the terms and conditions of the Creative Commons Attribution (CC BY) license (<https://creativecommons.org/licenses/by/4.0/>).

reduction (TPR), were employed to elucidate the structural and morphological properties. Enhanced basicity, metal–support interactions and oxygen vacancies were identified as possible factors affecting catalytic performance. These studies contribute to a better understanding of catalyst design principles and the optimization of DRM processes for sustainable biogas utilization, shedding light on future directions for hybrid biological/chemical H₂ production. One of the major drawbacks of this process is the formation of coke due to the following reactions:



It appears that whenever the oxygen species are missing, deposited carbon can stay on the surface of the catalyst and form a layer that covers the active metal or even diffuses through the particle to create a filament that separates the metal particles from the support [17]. Moreover, it was demonstrated that carbon deposition is favored by the presence of severe temperature gradients [18]. An effective way to avoid carbon deposition could therefore be to use a reactor that allows for suitable heat management. Among other solutions, e.g., fluidized beds [19], microreactors provide an interesting alternative because their small dimensions allow for high surface-to-volume ratios, which can enhance heat and mass transfer. Several studies have been carried out in small channels, mostly focusing on steam reforming [20–23]. Izquierdo et al. [24] performed a comparison of biogas oxidative reforming in a conventional reactor and in a microsystem. Although both configurations resulted in similar conversions, methane turnover frequency and hydrogen productivity were significantly larger in the microreactor. The present work focuses on the direct dry reforming of a model biogas on a Ru/Al₂O₃ catalyst in a microreactor composed of a pre-heating channel of 5 mm² width and 16 cm length, followed by a reaction square channel of 1 × 1 × 60 mm³; the catalyst is deposited at the bottom. When not specifically studying the performance of a catalyst, a commercial catalyst with a high ruthenium content is used.

Microreactors offer advantages over classical reactors like fixed and fluidized beds due to their miniature scale, enhanced mass and heat transfer rates, better control over reaction conditions and reduced residence time. In the presence of catalysts, their compact design enables the efficient utilization of space and resources, facilitating rapid reactions and improving the selectivity and yield of the desired products. Additionally, microreactors allow for the safer handling of hazardous chemicals and increase their scalability, making them ideal for diverse applications ranging from emulsification to the use of an anaerobic microreactor to intensify biogas production in our group [1]. The main objective is to demonstrate the feasibility of DRM in a microreactor through the simple contact between the model biogas circulating above the catalyst deposited at the bottom of the microchannel. This can drastically reduce the flow pattern, as seen in fixed or fluidized beds in previous studies.

2. Results and Discussions

2.1. Equilibrium Calculations

If no solid carbon is produced, the equilibrium conversions of methane and carbon dioxide for four values of CH₄:CO₂ are displayed in Figure 1.

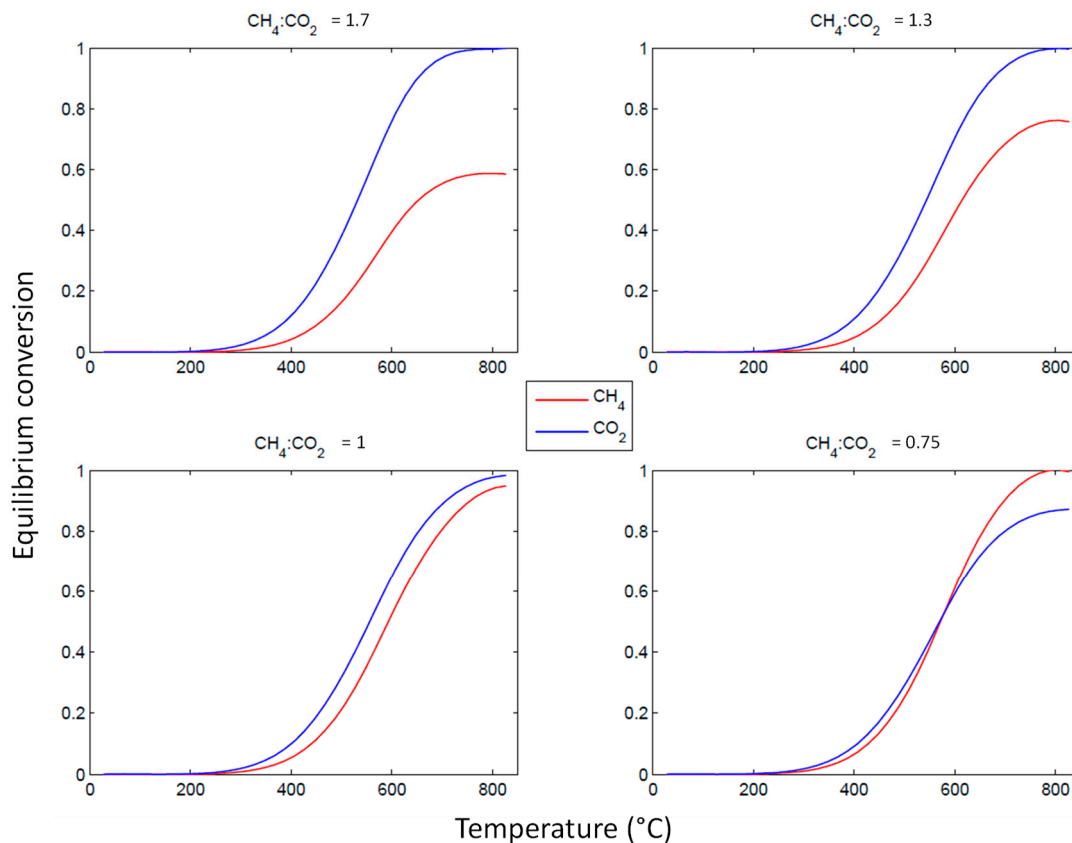


Figure 1. The equilibrium conversions of methane and carbon dioxide as a function of the temperature for various CH₄:CO₂ ratios when no solid carbon is formed under atmospheric pressure. The initial feed composition of CH₄:CO₂:N₂ is 18:18:64.

As expected, the conversions are very low if the temperature is lower than 400 °C. For higher temperatures, the reactants are consumed to produce hydrogen, carbon monoxide and water. When excess methane is present in the feed, its conversion rate is always smaller than that of carbon dioxide. Conversely, when carbon dioxide is in excess, X_{CH_4} is always better. To determine the equimolar composition of the feed, the conversion of carbon dioxide is slightly higher because of the reverse water–gas shift reaction:



If the formation of solid carbon is taken into account in the equilibrium calculations (Figure 2), the results are quite different. In this case, the reactants are converted even at low temperatures because of the reactions leading to carbon formation, as mentioned in Equations (2)–(5). When the temperature increases, the equilibria are reversed and the reforming reaction becomes predominant due to the necessary energy requirements. These results are similar to those obtained by other research groups [25,26].

Figure 2 shows the experimental values of X_{CH_4} and X_{CO_2} as a function of temperature for a CH₄:CO₂ ratio of 1.3 and a very low inlet volumetric flow rate of 20 mL·min⁻¹. These values are compared with those obtained by equilibrium calculations in the presence and absence of solid carbon, respectively. On one hand, it can be observed that the experimental data display a very satisfactory agreement with the equilibrium calculations in the absence of solid carbon. On the other hand, when carbon is added to the equilibrium calculations, the results are inconsistent for carbon dioxide since the experimental conversion cannot exceed the theoretical conversion.

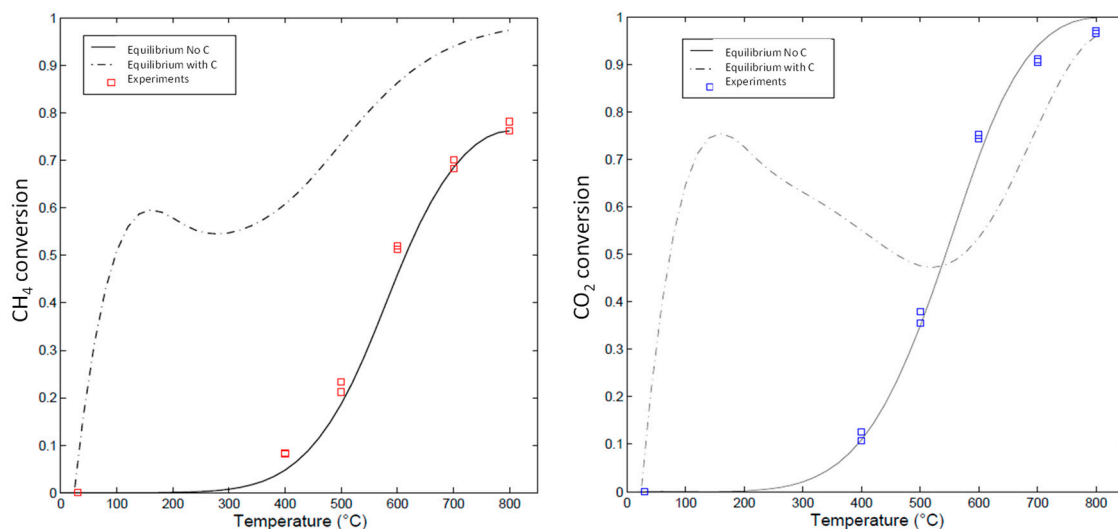


Figure 2. Comparison between experimental and equilibrium conversion rates of methane and carbon dioxide for a CH₄:CO₂ ratio of 1.3 and an inlet volumetric flow rate of 20 mL.min⁻¹.

The reasons for this behavior could be as follows: either the presence of other species not taken into account in the equilibrium calculations [27] or negligible carbon formation in our system due to the catalyst based on noble metals [28]. Certainly, the kind of catalyst used should play an important role in the carbon formation. Various oxidation methods could be employed to characterize the carbon balance in view of the catalyst's properties. The present work focuses only on the feasibility of biogas reforming, without focusing on the selection of a catalyst. This is supported by the fact that the elemental mass balance for carbon is almost always satisfied by the following equation:

$$F_{CH_4} + F_{CO_2} = F_{CH_4}^{out} + F_{CO_2}^{out} + F_{CO}^{out} \quad (7)$$

In fact, direct visual observations show no solid carbon formation in the microreactor after the experimental run. An additional explanation for this observation could be attributed to the diluted reaction feed, i.e., 64% nitrogen being present in the feed. The comparison shown in Figure 2 between the presence and absence of solid carbon confirms, without ambiguity, the absence of such a formation. Owing to the limited space size of the microreactor, the flow pattern should be quite close to ideal with respect to classical reactors with a bad fluid distribution passing through a catalyst fixed bed.

2.2. Effect of the Feed Flowrate

Along the microreactor, the total volumetric flow rate increases because the reforming reaction increases the number of moles in the gas mixture. The actual residence time is therefore different from the space time τ defined by the following:

$$\tau = V/Q \quad (8)$$

where V (m³) is the volume of the reactor and Q (m³/s) is the inlet volumetric flow rate. However, a variation of Q has the same effect on both the residence time and the space time. It is then possible to use the space time to analyze the behavior of the reaction system with respect to the influence of the feed flow rate. It is worth noting that, unlike a conventional fixed or fluidized catalytic bed, the catalyst is deposited at the bottom of the microchannel (cf. Section 3). The contact time between the gas and the catalyst is mainly localized at the surface layer of the catalyst, without penetrating the catalyst layer, considering the drop in pressure. Then, space time is employed here instead of the classical gas hourly space velocity (GHSV).

Respectively, Figures 3 and 4 display the values of the experimental conversion rates of methane and carbon dioxide as functions of either the gas flowrate at the inlet of the microreactor or the temperature for a $\text{CH}_4:\text{CO}_2$ ratio of 1. These equilibrium values with the space time τ under three different temperatures are in agreement with the expected trend: the conversion rates increase with the space time until they reach maximum conversion. This maximum conversion would indeed correspond to an infinite space time.

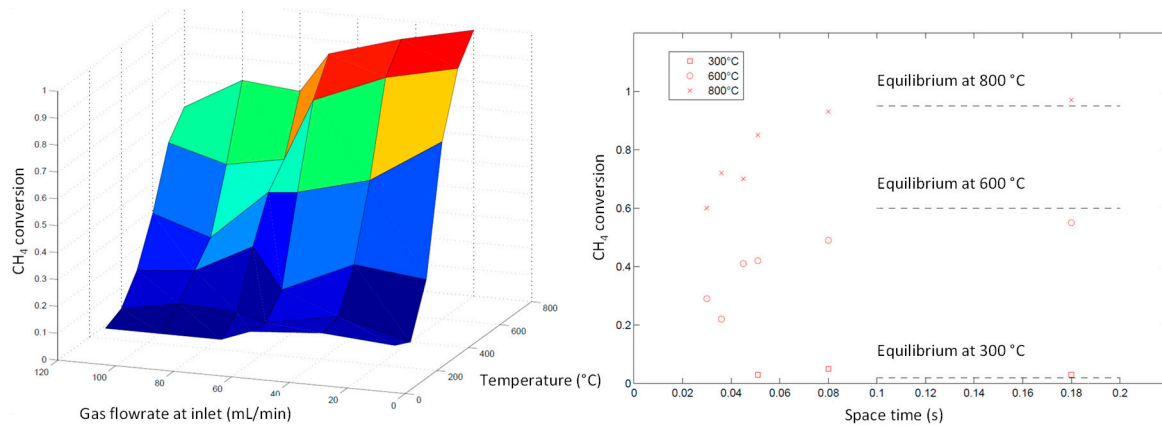


Figure 3. Experimental values of X_{CH_4} as a function of the space time compared to the equilibrium values for a $\text{CH}_4:\text{CO}_2$ ratio of 1.

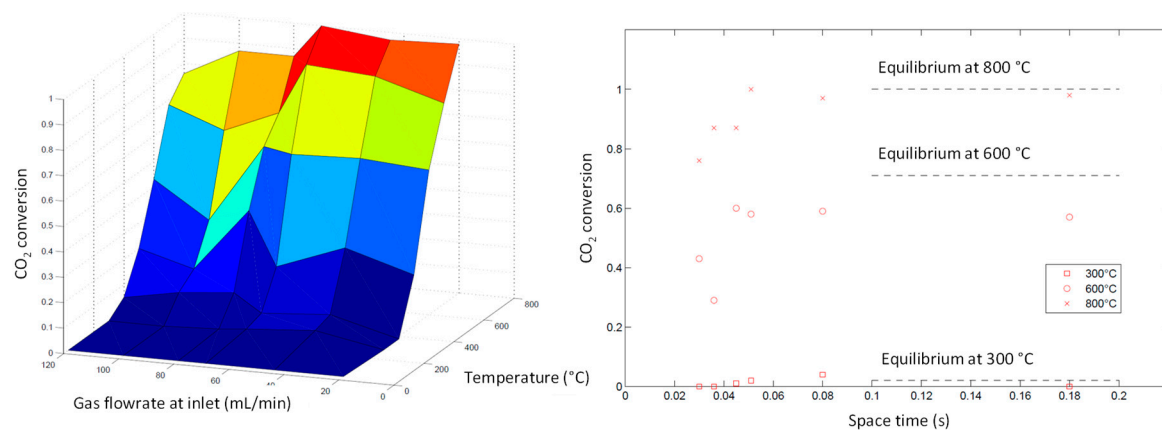


Figure 4. Experimental values of X_{CO_2} as a function of the space time compared to the equilibrium values for a $\text{CH}_4:\text{CO}_2$ ratio of 1.

The major result is that a short space time of 80 ms (volumetric flow rate of 45 $\text{mL}\cdot\text{min}^{-1}$) is sufficient to reach the maximum conversion for both reactants, even with only a superficial contact between the model biogas and the surface of the deposited catalyst in the microreactor.

2.3. Effect of the Feed Composition

Although the biogas composition is usually determined by the nature of the waste used in the anaerobic digestion process, the $\text{CH}_4:\text{CO}_2$ ratio in the biogas is of the utmost importance for the reforming reaction. As shown in Figure 5, the conversion rates of methane and carbon dioxide depend largely on this ratio. Since the feed inlet volumetric flow rate is 45 $\text{mL}\cdot\text{min}^{-1}$, these values are close to the equilibrium conversions. X_{CH_4} is close to 1 when methane is the limiting reactant but decreases rapidly when methane is in excess. Conversely, X_{CO_2} generally increases with the $\text{CH}_4:\text{CO}_2$ ratio. However, the trend is less clear because the reverse water–gas shift reaction (Equation (6)) also contributes to the conversion of carbon dioxide. For a typical biogas composition of $\text{CH}_4:\text{CO}_2 = 1.5$, a complete conversion of CH_4 would be impossible, even at high temperatures.

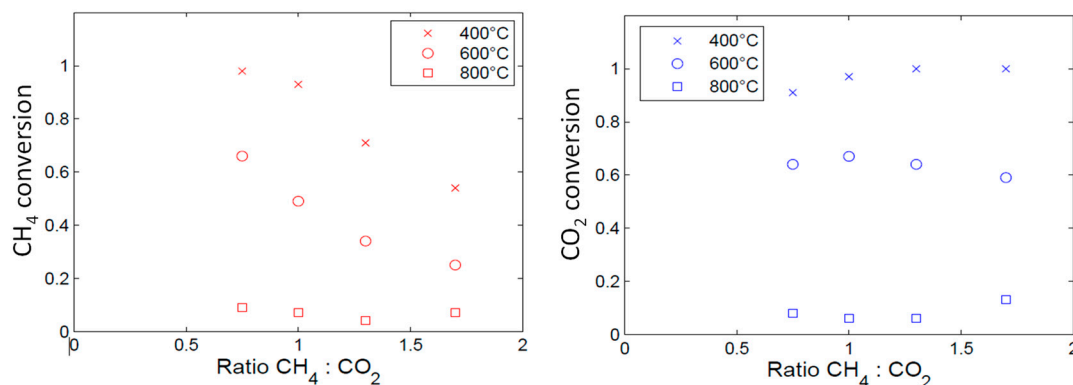


Figure 5. Experimental values of X_{CH_4} and X_{CO_2} as functions of $CH_4:CO_2$ ratio and temperature for a space time of 80 ms.

2.4. Product Distribution

The main products of the reaction are hydrogen and carbon monoxide. The distribution of these products is represented by the $H_2:CO$ ratio. This ratio is always inferior to 1 whereas the stoichiometry of the main reaction (Equation (1)) leads to a ratio equal to 1. This could be mainly attributed to the reverse water–gas shift reaction (Equation (6)), which converts hydrogen and carbon dioxide into water and carbon monoxide. Nevertheless, the endothermic character of this reaction implies a decrease in hydrogen consumption when temperature is increased. Measuring the amount of water produced would help to assess the importance of the reverse water–gas shift reaction. However, this was not possible in our system due to the very limited production of water in the microreactor. The gas mixture from the microreactor exit was sent to a heat exchanger in order to condense the water (cf. Section 3) and no water was collected there. A similar phenomenon was observed in another study of the dry methane reforming process [29], where it was attributed to the occurrence of the steam methane reforming reaction:



The consumption of hydrogen due to the in situ reduction in the catalyst might provide another explanation [30]. It is also noteworthy that these experimental values are in satisfactory agreement with the equilibrium calculations.

Moreover, Figure 6 reveals the variation in $H_2:CO$ in the function of $CH_4:CO_2$ at different temperatures for a given gas mixture flowrate of 45 mL/min. the $H_2:CO$ ratio increases with the $CH_4:CO_2$ ratio because of the increased availability of hydrogen atoms in this study. In the case of a real biogas ($CH_4:CO_2 = 1.5$), the $H_2:CO$ ratio could be as high as 0.85 at high temperatures according to this graph, without considering the impurities involved.

These results show that the direct biogas reforming is not an efficient way to produce large amounts of renewable hydrogen. But the process could be amended with a water–gas shift reactor after the reforming, as in the existing petroleum refineries for the production of hydrogen. The composition of the syngas could, however, be suitable for the production of liquid hydrocarbons by means of the Fischer–Tropsch process using an Fe-based catalyst [31] under certain conditions, such as a H_2/CO ratio notably higher than 1. Low- H_2/CO -ratio syngas can also be converted to higher alcohols using a Cu-based catalyst [32]. In addition, it is worth noting that, as observed with Pt- and Ni-based catalysts [33], the reforming observed here is mainly thermodynamically controlled.

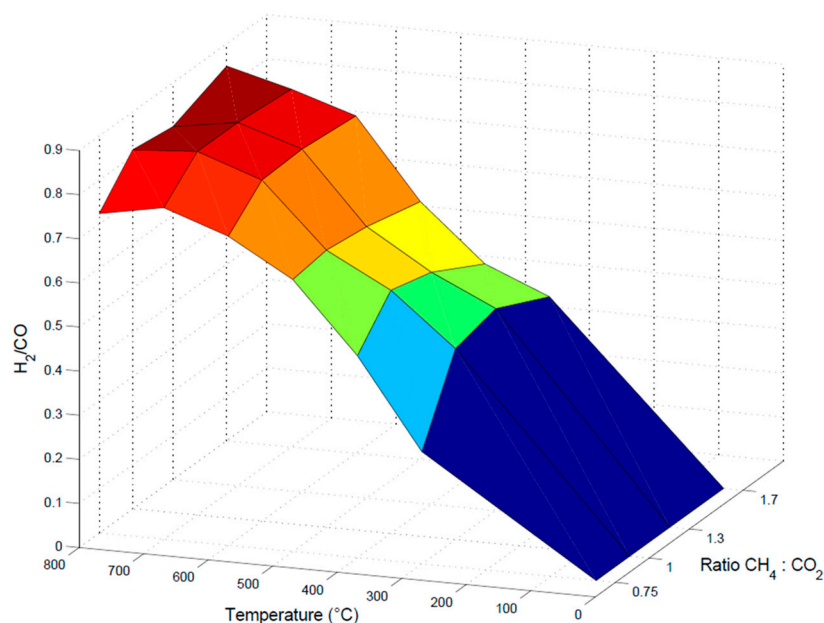


Figure 6. Variation in H₂:CO ratio with CH₄:CO₂ at different temperatures, with a total inlet volumetric flowrate of 45 mL.min⁻¹.

3. Materials and Methods

3.1. Catalyst Description

The catalyst used in the present work was purchased from Evonik Degussa GmbH (Evonik Noblyst® P3061 5% Ru, Sigma-Aldrich, Schnellendorf, Germany) and contains 5% wt. of ruthenium deposited on alumina. Such a high ruthenium content was chosen to guarantee an efficient conversion in order to test the feasibility of reforming. A basic characterization of the catalyst was carried out. The Sauter mean diameter of the catalyst particles was determined via laser granulometry (Malvern Mastersizer 2000, UK): $d_p = 28 \mu\text{m}$ over a range of 10 to 60 μm . The specific surface area S_{BET} was measured according to the adsorption of nitrogen using the B.E.T. method. The mean diameter of the internal pores d_{pore} and the specific surface S_{BET} were measured via the adsorption and desorption of nitrogen: $d_{pore} = 1.28 \times 10^{-8} \pm 1.0 \times 10^{-10} \text{ m}$ and $S_{BET} = 102 \pm 1 \text{ m}^2/\text{g}$. Both measurements were performed with an ASAP 2020 physisorption Analyzer (Micromeritics, Norcross, GA, USA). The shape of a catalyst particle is illustrated in Figure 7, as obtained by the SEM in our laboratory. The catalyst was not pre-treated before experiments. A fresh catalyst sample was employed each time a parameter was changed.

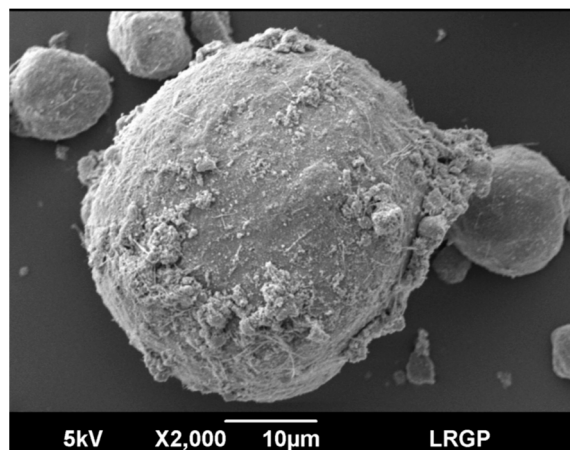


Figure 7. SEM image of a particle of Ru/Al₂O₃ catalyst.

3.2. Experimental Set-Up

The experimental set-up is presented in Figure 8. The first step is to mix pure methane and carbon dioxide (from two 3.5-grade gas bottles with a purity of 99.95%) in order to produce a gas mixture of the desired composition by means of two SLA5850 mass flow regulators (Brooks Instrument, Hatfield, PA, USA). The synthetic biogas is diluted in nitrogen and led into the microsystem. The total pressure is measured at both the inlet and the outlet of the regulator.

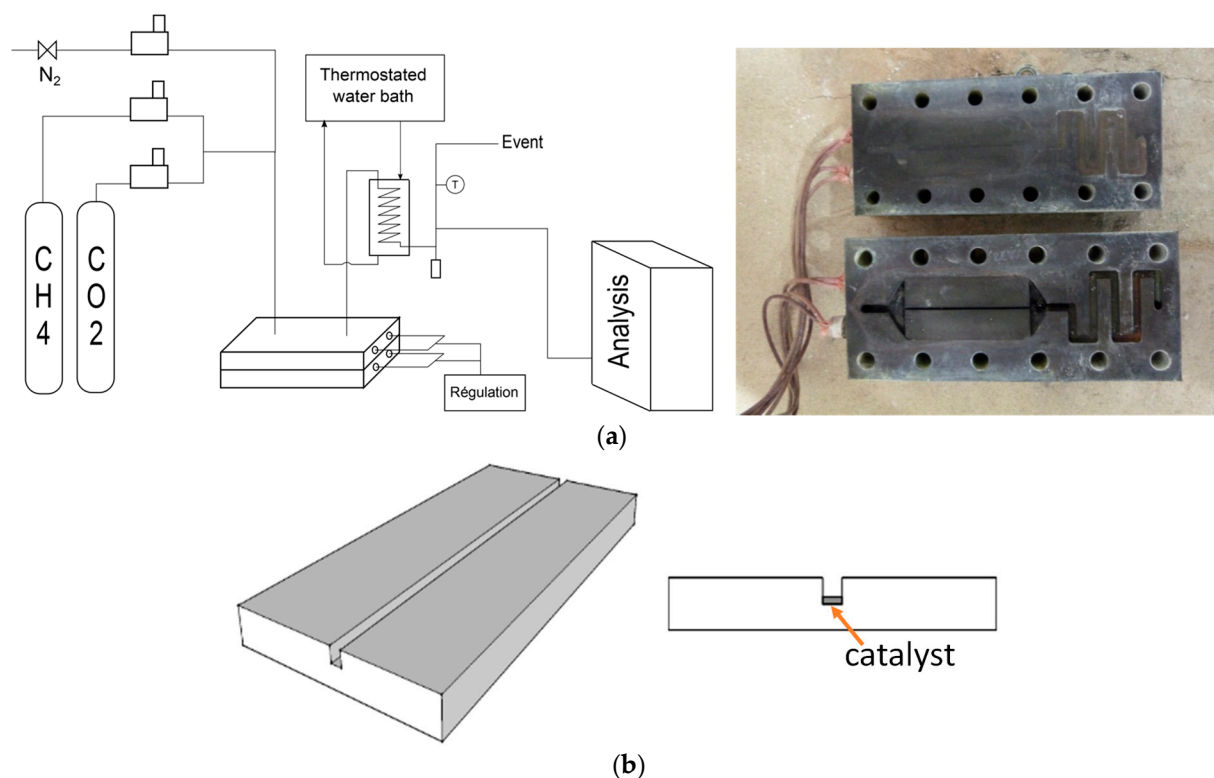


Figure 8. (a) Scheme of the experimental set-up (left) and picture of the microreactor (right). (b) Illustration of the channel of 1 mm height, 1 mm width and 60 mm length, with the catalyst deposited at the channel's bottom.

The microsystem is composed of two stainless steel plates, one of which was machined to create a channel for the pre-heating of gases and housing for the microchannel plate. The pre-heating channel has a section of 5 mm² and a total length of 16 cm. At the outlet of the pre-heating channel, the gas mixture enters the 1 × 1 × 60 mm³ square channel with the catalyst deposited at the bottom (cf. Figure 8b). The mass of the catalyst loaded in the reactor was 25 mg in every experiment. The gas mixture flows above the deposited catalyst particles without displacing them or carrying the finest ones, as was observed in a similar transparent channel at ambient temperature. For the experiments with a high temperature, the catalyst was regularly weighed and no significant loss was measured during the monitoring between the inlet and outlet of the microreactor. No pressure measurements were taken inside the microreactor along the flow as the pressure does not vary significantly.

At the end of the reaction zone, the gas mixture is sent to a heat exchanger in order to lower the temperature and condense the water. The composition is then measured by a gas chromatograph Micro GC 490 (Agilent Technologies, Santa Clara, CA, USA) equipped with thermal conductivity detector (TCD) and a CO_x column.

The tightness of the microreactor is tested in a water bath at ambient temperature. It should be noted that the gas mixture does not pass through a fixed catalyst bed as usual, which results in slight loss of pressure.

Each experiment was repeated three times, and this was extended to five times if a relative error above 5% was observed. The experimental error was around $\pm 5\%$. The influence of the following three parameters was investigated:

- The reactor temperature, which varied in the range 20–800 °C,
- The total inlet volumetric flowrate, which varied in the range 20–120 mL.min⁻¹,
- The composition of the feed, characterized by the CH₄:CO₂ ratio, which varied in the range 0.75–1.7.

Measurements of the outlet volumetric flow rate, along with the methane and carbon dioxide concentrations, are required for the calculation of conversion rates X_{CH_4} and X_{CO_2} :

$$X_{CH_4} = \frac{F_{CH_4} - F_{CH_4}^{out}}{F_{CH_4}} \quad (10)$$

$$X_{CO_2} = \frac{F_{CO_2} - F_{CO_2}^{out}}{F_{CO_2}} \quad (11)$$

where F_j and F_j^{out} are the molar flow rates of species j at the inlet and at the outlet of the microreactor, respectively.

3.3. Equilibrium Consideration

Chemical equilibrium calculations were essential to determine the maximum conversions of the reactants for a given feed composition and a given set of pressure and temperature conditions. The feed contains CH₄, CO₂ and N₂, and the major products are CO, H₂ and H₂O. The equilibrium concentrations were derived from the minimization of Gibbs energy under the constraints of the elemental mass balance. Two cases were investigated separately according to whether the formation of solid carbon was considered or not.

The Gibbs energy is a function of the N chemical potential of the various species:

$$G = \sum_{j=1}^N \mu_j n_j \quad (12)$$

The chemical potential of gases, treated like ideal gases, is expressed as follows:

$$\mu_j = \mu_j^0 + RT \ln(y_j) \quad (13)$$

where μ_j^0 is the chemical potential of the species j in the pure state.

At equilibrium, the chemical potential of carbon in the gas phase is equal to the chemical potential in the solid phase. The solid phase is assumed to be pure carbon; hence, the chemical potential of carbon is equal to zero.

3.4. Assessment of Diffusional Limitation

In order to elucidate the true effect of the experimental parameters on the reactants' conversion and the reaction rates, it is necessary to assess the eventual diffusional limitations. Firstly, there is a concentration gradient in the channel over the catalyst layer because the flow is in the laminar regime (the Reynolds number based on the hydraulic diameter is lower than 60). However, the maximum diffusion time t^{diff} in the gas phase, calculated with Equation (14), is always smaller than the residence time. Except for very short residence times, the concentration gradient in the channel can therefore be neglected.

$$t_j^{diff} = \frac{h^2}{D_j} \quad (14)$$

where h (m) is the height of the channel (1 mm) and D_j (m².s⁻¹) is the diffusivity of species j estimated from [34].

Secondly, the external mass transfer limitations could be assessed. The concentration gradient around a catalyst particle can be derived from the steady-state mass balance on species j :

$$k_D (C_j^e - C_j^s) A_p = r_j V_p \quad (15)$$

where k_D ($\text{m}\cdot\text{s}^{-1}$) is the mass transfer coefficient, C_j^e and C_j^s ($\text{mol}\cdot\text{m}^{-3}$) are the molar concentration of species j outside the diffusion film and at the surface of the particle, respectively, A_p (m^2) and V_p (m^3) are the surface and volume of the particle and r_j ($\text{mol}\cdot\text{m}^{-3}\cdot\text{s}^{-1}$) is the apparent reaction rate of species j .

The mass transfer coefficient k_D can be estimated using a standard correlation [35]:

$$Sh = \frac{k_D d_p}{D_j} = 2 + 1.8 Re^{1/2} Sc^{1/3} \quad (16)$$

where Sh is the Sherwood number, d_p (m) is the diameter of the catalyst particles, Re is the Reynolds number and Sc is the Schmidt number.

The fraction of external mass transfer limitation is defined using the hypothesis of a spherical catalyst particle:

$$f_e = \frac{(C_j^e - C_j^s)}{C_j^e} = \frac{r_j d_p}{6 k_D C_j^e} \quad (17)$$

The results are presented in Table 1 under the following conditions: inlet volumetric flowrate of $100 \text{ mL}\cdot\text{min}^{-1}$; temperature of $700 \text{ }^\circ\text{C}$. The apparent reaction rate of both reactants measured is smaller than $400 \text{ mol}\cdot\text{m}^{-3}\cdot\text{s}^{-1}$ under these conditions. Therefore, using this value in the calculations could only lead to an overestimation of f_e . As illustrated in Table 1, the external mass transfer limitations are also negligible.

Table 1. Estimation of the fraction of external mass transfer limitations.

Species	D ($\text{m}^2\cdot\text{s}^{-1}$)	Re	Sc	Sh	k_D ($\text{m}\cdot\text{s}^{-1}$)	C_j^e ($\text{mol}\cdot\text{m}^{-3}$)	f_e
CH ₄	7.46×10^{-5}	0.38	1	3.1	14	3.9	2.10×10^{-5}
CO ₂	1.07×10^{-5}	0.38	1.4	3.2	10	3.7	3.10×10^{-5}

Finally, internal mass transfer limitations are assessed using a Thiele modulus Φ , which compares the maximum reaction rate to the diffusion rate of a reactant:

$$\Phi = \frac{r_j d_p^2}{36 C_j^s D^f} \quad (18)$$

where D^f (m^2/s) is the effective diffusivity, defined as follows:

$$D^f = \frac{\epsilon D}{\tau_p} \quad (19)$$

where ϵ is the internal porosity of the particle and τ_p is its tortuosity. For an alumina catalyst, typical values of these parameters would be $\epsilon = 0.5$ and $\tau_p = 7.5$ [36]. The diffusivity D needs to be replaced by Knudsen diffusivity because the mean free path of the reactants is around $2 \times 10^{-7} \text{ m}$, whereas the diameter of the pores is less than $2 \times 10^{-8} \text{ m}$. It is worth noting that this estimation only provides an order of magnitude, without quantifying the diffusional limitation within our microreactor. In fact, the microreactor used here has a channel with only a partially loaded catalyst at the bottom, unlike a classical fixed-catalytic-bed reactor at the macroscale, with gases flowing across the whole section. In the present microreactor, the reforming would mainly take place at the surface of the catalyst layers in direct contact with the gases.

The results are presented in Table 2 for the following conditions: inlet volumetric flowrate of $100 \text{ mL}\cdot\text{min}^{-1}$ and temperature of $700 \text{ }^\circ\text{C}$. Under these conditions, the apparent reaction rate of both the measured reactants is smaller than $400 \text{ mol}\cdot\text{m}^{-3}\cdot\text{s}^{-1}$. Therefore, using this value in the calculations could only lead to an overestimation of Φ . These data reveal that the Thiele modulus is significantly smaller than 1. This means that internal transfer is not a limiting factor for the mass transfer.

Table 2. Estimation of the Thiele modulus Φ .

Species	$D \text{ (m}^2\cdot\text{s}^{-1}\text{)}$	$C_j^s \text{ (mol}\cdot\text{m}^{-3}\text{)}$	Φ
CH ₄	1.11×10^{-8}	3.9	0.07
CO ₂	6.73×10^{-9}	3.7	0.12

Obviously, no part of the mass transfer process is subject to diffusional limitations. This is mainly due to the fact that both the microreactor dimensions and the catalyst particle are small enough. Consequently, the performance of the microreactor is only limited by the reaction rate, and the kinetics measured in this work faithfully reflect the intrinsic kinetics. As expected, the microreactor provides quasi-perfect conditions to achieve conversion results that are close to equilibrium. Complex flow patterns will certainly affect the conversion efficiency in classical catalytic reactors like fixed beds.

4. Conclusions

The direct dry reforming of a simplified model biogas over a Ru/Al₂O₃ catalyst was experimentally investigated. The reaction took place in a narrow channel to avoid diffusional mass transfer limitations and to assure high reaction rates. The best operating conditions seem to be a space time of 80 ms, a temperature of $700 \text{ }^\circ\text{C}$ and a CH₄:CO₂ ratio close to unity. Of course, this conclusion should be moderated as the results were close to the equilibrium curve under the particular conditions of the microreactor. This work mainly focused on the feasibility of DRM in a microreactor. The excess Ru load of a Ru-based catalyst was chosen to guarantee the total conversion of methane at the outlet of the microreactor within a very short space time. These results could pave the way for processing real biogas reforming in the presence of impurities like ammonia and hydrogen sulfide. The choice of a realistic catalyst and an intensified microreactor design requires further investigation.

Author Contributions: Conceptualization, T.N.W., J.W. and H.Z.L.; methodology, T.N.W. and H.Z.L.; validation, T.N.W., J.W. and H.Z.L.; formal analysis, T.N.W. and H.Z.L.; investigation, T.N.W., J.W. and H.Z.L.; resources, J.W. and H.Z.L.; data curation, T.N.W. and H.Z.L.; writing—original draft preparation, T.N.W. and H.Z.L.; writing—review and editing, T.N.W., J.W. and H.Z.L.; supervision, J.W. and H.Z.L.; project administration, J.W. and H.Z.L.; funding acquisition, J.W. and H.Z.L. All authors have read and agreed to the published version of the manuscript.

Funding: This research was funded by the French Agence Nationale de la Recherche (ANR-10-INTB-0906 PROMET) and by the Natural Science Foundation of China (51061130555).

Institutional Review Board Statement: Not applicable.

Informed Consent Statement: Not applicable.

Data Availability Statement: Related data could be made available upon request.

Acknowledgments: The valuable comments and constructive suggestions of the Reviewers and Editors are gratefully acknowledged.

Conflicts of Interest: The authors declare no conflicts of interest.

References

1. Zhang, J.B.; Wu, J.; Poncin, S.; Hamelin, M.; Li, H.Z. Microscale study of anaerobic biogas production under various hydrodynamic conditions. *Environ. Sci. Technol.* **2012**, *46*, 8698–8704. [[CrossRef](#)] [[PubMed](#)]
2. Wedraogo, T.N.; Poncin, S.; Wu, J.; Li, H.Z. Intensified biogas purification in a stirred tank. *Chem. Eng. Process.* **2014**, *86*, 1–8. [[CrossRef](#)]
3. Hu, Y.Y.; Wu, J.; Poncin, S.; Cao, Z.P.; Li, Z.H.; Li, H.Z. Flow field investigation of high solid anaerobic digestion by Particle Image Velocimetry (PIV). *Sci. Total Environ.* **2018**, *626*, 592–602. [[CrossRef](#)] [[PubMed](#)]
4. Hu, Y.Y.; Zhang, S.; Wang, X.; Peng, X.; Hu, F.; Dai, H.; Wu, J.; Poncin, S.; Li, H.Z. Visualization of mass transfer in mixing processes of high solid anaerobic digestion using Laser Induced Fluorescence (LIF) technique. *Waste Manag.* **2021**, *127*, 121–129. [[CrossRef](#)] [[PubMed](#)]
5. Hu, Y.Y.; Zheng, X.; Zhang, S.; Ye, W.; Wu, J.; Poncin, S.; Li, H.Z. Investigation of hydrodynamics in high solid anaerobic digestion by particle image velocimetry and computational fluid dynamics: Role of mixing on flow field and dead zone reduction. *Bioresour. Technol.* **2021**, *319*, 124130. [[CrossRef](#)]
6. Zhao, X.; Joseph, B.; Kuhn, J.; Ozcan, S. Biogas reforming to syngas: A review. *iScience* **2020**, *23*, 101082. [[CrossRef](#)]
7. Le Saché, E.; Moreno, A.A.; Reina, T.R. Biogas conversion to syngas using advanced Ni-promoted pyrochlore catalysts: Effect of the CH₄/CO₂ ratio. *Front. Chem.* **2021**, *9*, 672419. [[CrossRef](#)] [[PubMed](#)]
8. Jung, S.; Lee, J.; Moon, D.Y.; Kim, K.Y.; Kwon, E.E. Upgrading biogas into syngas through dry reforming. *Renew. Sustain. Energy Rev.* **2021**, *143*, 110949. [[CrossRef](#)]
9. Kumar, R.; Kumar, A.; Pal, A. Simulation modelling of hydrogen production from steam reforming of methane and biogas. *Fuel* **2024**, *362*, 130742. [[CrossRef](#)]
10. Rostrup-Nielsen, J.R.; Hansen, J.H.B. CO₂-Reforming of methane over transition metals. *J. Catal.* **1993**, *144*, 38–49. [[CrossRef](#)]
11. Charisiou, D.; Siakavelas, G.; Papageridis, K.N.; Baklavariadis, A.; Tzounis, L.; Avraam, D.G.; Goula, M.A. Syngas production via the biogas dry reforming reaction over nickel supported on modified with CeO₂ and/or La₂O₃ alumina catalysts. *J. Nat. Gas Sci. Eng.* **2016**, *31*, 164–183. [[CrossRef](#)]
12. Chava, R.; Seriyala, K.A.; Varma, D.B.A.; Eluvu, K.; Roy, B.; Appari, S. Investigation of Ba doping in A-site deficient perovskite Ni-exsolved catalysts for biogas dry reforming. *Int. J. Hydrogen Energy* **2023**, *48*, 27652–27670. [[CrossRef](#)]
13. Latsiou, A.I.; Bereketidou, O.A.; Charisiou, N.D.; Georgiadis, A.G.; Avraam, D.G.; Goula, M.A. Synthesis and Mathematical Modelling of the Preparation Process of Nickel-Alumina Catalysts with Egg-Shell Structures for Syngas Production via Reforming of Clean Model Biogas. *Catalysts* **2022**, *12*, 274. [[CrossRef](#)]
14. Chaghouri, M.; Hany, S.; Cazier, F.; Tidahy, H.L.; Gennequin, C.; Abi-Aad, E. Impact of impurities on biogas valorization through dry reforming of methane reaction. *Int. J. Hydrogen Energy* **2022**, *47*, 40415–40429. [[CrossRef](#)]
15. Moogi, S.; Ko, C.H.; Rhee, G.H.; Jeon, B.H.; Khan, M.A.; Park, Y.K. Influence of catalyst synthesis methods on anti-coking strength of perovskites derived catalysts in biogas dry reforming for syngas production. *Chem. Eng. J.* **2022**, *437*, 135348. [[CrossRef](#)]
16. Strniša, F.; Sagar, V.T.; Djinović, P.; Pintar, A.; Plazl, I. Ni-containing CeO₂ rods for dry reforming of methane: Activity tests and a multiscale lattice Boltzmann model analysis in two model geometries. *Chem. Eng. J.* **2021**, *413*, 127498. [[CrossRef](#)]
17. Kroll, V.C.H.; Swaan, H.M.; Mirodatos, C. Methane reforming reaction with carbon dioxide over Ni/SiO₂ catalyst: I. Deactivation Studies. *J. Catal.* **1996**, *161*, 409–422. [[CrossRef](#)]
18. Abdulrasheed, A.; Jalil, A.A.; Gambo, Y.; Ibrahim, M.; Hambali, H.U.; Shahul Hamid, M.Y. A review on catalyst development for dry reforming of methane to syngas: Recent advances. *Renew. Sustain. Energy Rev.* **2019**, *108*, 175–193. [[CrossRef](#)]
19. Al-Otaibi, F.N.; Berrouk, A.S.; Xiao, X. Analysis of dry reforming of methane under different fluidization regimes using a multiphase particle-in-cell approach. *Phys Fluids.* **2023**, *35*, 033327. [[CrossRef](#)]
20. Simsek, E.; Avci, A.K.; Önsan, Z.I. Investigation of catalyst performance and microstructured reactor configuration for syngas production by methane steam reforming. *Catal. Today* **2011**, *178*, 157–163. [[CrossRef](#)]
21. Mbodji, M.; Commenge, J.M.; Falk, L.; Di Marco, D.; Rossignol, F.; Prost, L.; Valentin, S.; Joly, R.; Del-Gallo, P. Steam methane reforming reaction process intensification by using a millistructured reactor: Experimental setup and model validation for global kinetic reaction rate estimation. *Chem. Eng. J.* **2012**, *207*, 871–884. [[CrossRef](#)]
22. Karakaya, M.; Keskin, S.; Avci, A.K. Parametric study of methane steam reforming to syngas in a catalytic microchannel reactor. *Appl. Catal. Gen.* **2012**, *411*, 114–122. [[CrossRef](#)]
23. Chen, J.; Song, W.; Xu, D. Compact steam-methane reforming for the production of hydrogen in continuous flow microreactor systems. *ACS Omega* **2019**, *4*, 15600–15614. [[CrossRef](#)] [[PubMed](#)]
24. Izquierdo, U.; Barrio, V.L.; Lago, N.; Requies, J.; Cambra, J.F.; Güemez, M.B.; Arias, P.L. Biogas steam and oxidative reforming processes for synthesis gas and hydrogen production in conventional and microreactor reaction systems. *Int. J. Hydrogen Energy* **2012**, *37*, 13829–13842. [[CrossRef](#)]
25. Pinilla, J.L.; de Llobet, S.; Suelves, I.; Utrilla, R.; Lázaro, M.J.; Moliner, R. Catalytic decomposition of methane and methane/CO₂ mixtures to produce synthesis gas and nanostructured carbonaceous material. *Fuel* **2011**, *90*, 2245–2253. [[CrossRef](#)]
26. Muradov, N.; Smith, F.; T-Raissi, A. Hydrogen production by catalytic processing of renewable methane-rich gases. *Int. J. Hydrogen Energy* **2008**, *33*, 2023–2035. [[CrossRef](#)]
27. Nikoo, M.K.; Amin, N.A.S. Thermodynamic analysis of carbon dioxide reforming of methane in view of solid carbon formation. *Fuel Process. Technol.* **2011**, *92*, 678–691. [[CrossRef](#)]

28. Pakhare, D.; Spivey, J. A review of dry (CO₂) reforming of methane over noble metal catalysts. *Chem. Soc. Rev.* **2014**, *43*, 7813–7837. [[CrossRef](#)]
29. Serrano-Lotina, A.; Daza, L. Influence of the operating parameters over dry reforming of methane to syngas. *Int. J. Hydrogen Energy* **2014**, *39*, 4089–4094. [[CrossRef](#)]
30. Daza, C.E.; Kiennemann, A.; Moreno, S.; Molina, R. Dry reforming of methane using Ni–Ce catalysts supported on a modified mineral clay. *Appl. Catal. Gen.* **2009**, *364*, 65–74. [[CrossRef](#)]
31. Davis, B.H. Fischer-Tropsch synthesis: Relationship between iron catalyst composition and process variables. *Catal. Today* **2003**, *84*, 83–98. [[CrossRef](#)]
32. Gupta, M.; Smith, M.L.; Spivey, J.J. Heterogeneous Catalytic Conversion of Dry Syngas to Ethanol and Higher Alcohols on Cu-Based Catalysts. *ACS Catal.* **2011**, *1*, 641–656. [[CrossRef](#)]
33. García-Diéguez, M.; Pieta, I.S.; Herrera, M.C.; Larrubia, M.A.; Alemany, L.J. Nanostructured Pt- and Ni-based catalysts for CO₂-reforming of methane. *J. Catal.* **2010**, *270*, 136–145. [[CrossRef](#)]
34. Reid, R.C.; Prausnitz, J.M.; Sherwood, T.K. *The Properties of Gases and Liquids*; McGraw-Hill chemical engineering series; McGraw-Hill: New York, NY, USA, 2001.
35. Kunii, D.; Levenspiel, O. *Fluidization Engineering*; Wiley: New York, NY, USA, 1969.
36. Villermaux, J. *Génie de la Réaction Chimique: Conception et Fonctionnement des Réacteurs*; Tec & Doc: Pairs, France, 1993.

Disclaimer/Publisher’s Note: The statements, opinions and data contained in all publications are solely those of the individual author(s) and contributor(s) and not of MDPI and/or the editor(s). MDPI and/or the editor(s) disclaim responsibility for any injury to people or property resulting from any ideas, methods, instructions or products referred to in the content.